NASA

Technical Memorandum 86077

Submillimeter Wavelength Survey of the Galactic Plane from $\ell = -5°$ to $\ell = +62°$: Structure and Energetics of the Inner Disk

M. G. Hauser, R. F. Silverberg, M. T. Stier, T. Kelsall, D. Y. Gezari, E. Dwek, D. Walser, J. C. Mather, and L. H. Cheung

MARCH 1984

National Aeronautics and Space Administration

Goddard Space Flight Center
Greenbelt, Maryland 20771

SUBMILLIMETER WAVELENGTH SURVEY OF THE GALACTIC PLANE FROM $\ell = -5^{\circ}$ to $\ell = +62^{\circ}$: STRUCTURE AND ENERGETICS OF THE INNER DISK

M. G. HAUSER, R. F. SILVERBERG, M. T. STIER,[1] T. KELSALL, D. Y. GEZARI, E. DWEK,[1] D. WALSER, J. C. MATHER

Laboratory for Extraterrestrial Physics

Goddard Space Flight Center

and

L. H. CHEUNG

Department of Physics and Astronomy

University of Maryland

Received_____; accepted_____

[1]NAS-NRC Resident Research Associate

ABSTRACT

We present results from a new large-scale survey of the first quadrant of the galactic plane at wavelengths of 150, 250, and 300 μm, with a 10x10 arcmin beam. The emission detected in the survey arises from compact sources, most of which are identified with known peaks of 5 GHz and/or CO emission, and from an underlying diffuse background with a typical angular width of $\sim 0.9^{\circ}$ (FWHM) which accounts for most of the emission. A total of 80 prominent discrete sources are identified and characterized, of which about half have not previously been reported at far infrared wavelengths. The total infrared luminosity within the solar circle is $\sim 1\text{-}2\times10^{10}$ $L_{\odot}$, and is probably emitted by dust that resides in molecular clouds.

I. INTRODUCTION

Over the last decade, it has become apparent that a large number of galactic and extragalactic objects emit a significant fraction of their total luminosity at far infrared (FIR) and submillimeter (SMM) wavelengths. Some objects are so cool that they may be only observable at SMM wavelengths (Gezari 1982). While many observations of the Galaxy have already been made at FIR/SMM wavelengths (for a summary see Okuda 1981), most of these have covered only a small fraction of the plane with relatively large beam systems.

We have developed and flown a new 1.2m diameter balloon-borne telescope (Silverberg et al. 1979, 1983) to survey the galactic plane at FIR/SMM wavelengths. In this paper we present survey data extending from $l=-5$ to $l=62^{\circ}$ in galactic longitude for latitudes in the range $-3^{\circ} \lesssim b \lesssim +3^{\circ}$. Preliminary discussions of portions of these data have been presented elsewhere (Cheung 1980; Stier et al. 1982; Hauser et al. 1983). This region has been observed in whole or in part by several other groups at various FIR/SMM wavelengths; for example, Hoffmann, Frederick, and Emery (1971), Low et al. (1977), Emerson, Jennings, and Moorwood (1973), Serra et al. (1978 and 1979), Owens, Muehlner, and Weiss (1979), Viallefond, et al. (1980), Nishimura, Low, and Kurtz (1980), Maihara, Oda, and Okuda

(1979), Maihara et al. (1981), Boissé et al. (1981), and Gispert, Puget, and Serra (1982). Distinguishing features of this survey include high sensitivity, three low-pass spectral bands to permit inference of both temperature and density information, and 10-arcmin spatial resolution to provide detailed information on discrete regions as well as the large-scale diffuse emission.

The primary objectives of this survey are to map the spatial distribution of interstellar material and its heating sources within the Galaxy, to determine physical conditions such as temperature, optical depth, mass column density, and luminosity in discrete galactic sources, and to explore the variation of those conditions on a large scale. The radiation detected in the FIR/SMM wavelength region is consistent with thermal emission from dust grains. Although the dust constitutes a minor fraction ($\lesssim 0.01$) of the mass, it has a major effect on the energy balance and gas phase chemical composition of the interstellar medium. Since the dust is an inefficient absorber at FIR/SMM wavelengths, direct observation at these wavelengths reveals the distribution of the dust throughout the Galaxy.

The instrumental and observational details are briefly described in section II. The survey data show that the FIR/SMM emission from the inner regions of the galactic plane arises from

two distinct components: discrete sources and an underlying extended emission component. The observations and the analysis of the physical conditions of the dust in each of the components are presented in section III. In section IV we compare the results of this survey with CO and radio continuum surveys of similar regions of the galactic plane. The origin of the diffuse component of the FIR/SMM emission from the galactic plane is discussed in section V, and a brief summary of results is given in section VI.

II. INSTRUMENTATION AND OBSERVATIONS

The main components of the balloon-borne submillimeter observatory are an altitude/azimuth-mounted 1.2-meter (48-inch) diameter Cassegrain telescope with servo-controlled chopping secondary mirror, and a liquid-helium cooled filter photometer. The photometer contains composite germanium bolometer detectors operating in three low-pass spectral bands with effective wavelengths of approximately 150 μm, 250 μm, and 300 μm. A microprocessor-based electronics system is used to control the telescope and the experiment electronics. The scientific and housekeeping data are transmitted to the ground in real time. A detailed description of the telescope, detector system, and gondola instrumentation has been given by Silverberg et al. (1979, 1983) and Cheung (1980).

The SMM observatory was launched from the National Scientific Balloon Facility at Palestine, Texas. Three successful flights were completed in November 1979, August 1980, and September 1982 (hereafter designated as flights 1, 2, and 3 respectively), providing a total of $\sim$ 21 hours of useable data at a float altitude of 30 km. Regions of the sky observed during the first two flights, from which the data presented here were obtained, are shown in Figure 1.

The basic observational parameters of the system are summarized in Table 1. Normalized transmission curves for the filters, measured with a Fourier transform spectrometer, are shown in Figure 2. Observations are made by raster-scanning the array of three bolometers, whose fields of view are separated by 17 arcmin perpendicular to the scan direction. The chopper throw, 20 arcmin peak-peak, is in the scan direction. The chopper has a square waveform with an $\sim$ 80% duty cycle. Each region of the sky is observed three times, once in each of the three detector channels during sequential raster lines.

Jupiter was observed during flight 1 for photometric calibration, but was not successfully observed during flight 2. M17, however, was observed during both flights 1 and 2, and has

been used here as a secondary calibrator to transfer the flight 1 calibration to flight 2 data. Since the cut-on wavelength for band 2 was somewhat different in the two flights (see Table 1 and Figure 2), a spectral shape for M17 had to be adopted. A 33 K Planck curve modified by a λ^{-2} emissivity law, consistent with the flight 1 measurements, was used for this purpose. The Jupiter brightness temperature was taken to be 125 K in all bands (Wright, 1976). The estimated accuracy of the photometric scale is $\sim$ 50% for both point and extended sources. The predominant cause of this uncertainty is lack of precise knowledge of both the beam shape and the cross-scan position of the calibration source when it transited the beam.

Attitude reconstruction is made after the flight by comparing records of a magnetometer, a Si photodiode visible-light star sensor mounted in the focal plane, an aspect camera, and a two-axis inertial gyroscope aligned with the telescope. The procedure used is to identify visible stars detected by the Si photodiode and the camera, and to use these sightings to determine any offsets in the magnetometer and gyroscope signals. Offsets from the SMM detectors to the visible detector are determined from planet crossings. The resulting positional accuracy of this procedure is typically 4 arcmin rms. This is established from multiple star sightings and positional correlation of compact SMM sources with known HII regions.

The signal from each detector was synchronously demodulated in the ground data processing using digital filtering. The synchronously demodulated output was deconvolved for the effects of beam switching on extended sources using Simon's algorithm (Simon, 1976). The deconvolution process reduces the signal-to-noise ratio so that, even for point sources, parameters derived from the map data may differ somewhat from those obtained directly from the synchronously-demodulated data. Detailed discussions of data analysis procedures are given by Silverberg et al. (1979) and Cheung (1980).

III. THE COMPONENTS OF THE FIR/SMM EMISSION

Maps of the FIR/SMM surface brightness of the galactic plane in the three survey bands are shown in Figure 3. These maps reveal nearly continuous diffuse emission from the inner Galaxy, as well as emission from prominent compact sources. Most of these compact sources can be identified with known HII regions. In this paper, we concentrate on the emission from the $10^{\circ} \leq \ell \leq 45^{\circ}$ region of the galactic plane. A detailed discussion of the compact sources and their association with HII regions and molecular clouds is given by Myers et al. (1984). A preliminary discussion of the galactic center region has been presented separately (Stier et al., 1982).

All of the FIR/SMM continuum emission mapped in this survey is attributed to thermal emission from interstellar dust. We first present an analysis of the longitudinal profiles of the emission in the various survey bands averaged over $\pm$ 0.5^{o} in latitude. Estimating a smooth background level from the contour maps we find that the discrete sources contribute on the average less than 20 percent to the emission integrated over this latitude range. The longitudinal brightness profiles and derived physical quantities therefore represent on the average the brightness and physical conditions of the dust that gives rise to the diffuse emission from the galactic plane. In the analysis of the compact sources, no attempt is made here to separate the sources from the background. The physical parameters of the dust in the sources are therefore derived from peak flux data because these are least contaminated by the underlying diffuse emission.

To estimate the physical conditions of the dust, it is assumed that the composition and the physical properties (optical constants, size distribution) of the dust particles do not vary with longitude, and that all of the interstellar dust along a given line of sight participates in the emission at the same characteristic line-of-sight dust temperature. The derived temperature therefore represents a mean temperature on scales corresponding to the beam size.

a) Diffuse Emission Component

(i) Intensity variation with longitude

Longitudinal profiles of the FIR/SMM surface brightness in the galactic plane are shown in Figure 4. These profiles show the brightness variations of the emission in longitudinal increments of 6 arcmin, averaged over ± 0.5 degrees in galactic latitude centered on the galactic plane. The brightness profiles show significant structure resulting from some large scale concentration of the emission in the Galaxy, and, in a few cases, from the contribution of strong discrete sources. The profiles exhibit a general trend of decreasing brightness with increasing galactic longitude. The conversion from the in-band observed intensity in W m^{-2} sr^{-1} to specific intensity in Jy sr^{-1} (= 10^{-26} W m^{-2} Hz^{-1} sr^{-1}) was done assuming a 25 K source temperature and a λ^{-2} emissivity law, giving the effective filter bandwidths shown in Table 1.

(ii) Intensity variation with latitude

The distribution of the emission in latitude has a characteristic width of $\sim 0.9^{\circ}$ (FWHM) corresponding to a scale height of 80 pc for a source distance of 7 kpc. This scale height is characteristic of the spiral arm population, consisting primarily of molecular clouds, OB, T Tauri, and supergiant stars, and some members of the young disk population, primarily A stars

(Mihalas and Binney 1981). This scale height is also comparable to that of the extended low density HII region (Westerhout 1958). Typical scale heights of the intermediate and oldest disk population is >400 pc, showing that the FIR emission is clearly associated with the young galactic components.

(iii) Dust spectral index

At FIR/SMM wavelengths, the radiative efficiency, or, equivalently, the mass absorption coefficient, $K(\lambda)$, of the dust, can be characterized by a power-law dependence on wavelength λ, $K(\lambda) \propto \lambda^{-n}$. This survey was made in three spectral bands, chosen so that both the spectral index, n, and the dust temperature, T, could be independently determined from high signal-to-noise ratio observations. Unfortunately, a technical problem in the first flight caused the effective wavelengths of bands 2 and 3 to be more similar than intended, making an independent determination of n and T impossible. We therefore have adopted a nominal value of n=2 for the emissivity index of the dust. This value represents the theoretical long-wavelength behavior of $K(\lambda)$ in a simple oscillator model for the absorption (e.g. Andriesse 1974), and is about equal to the average value of the emissivity index of both graphite and silicate grains over the 100-1000 μm wavelength interval (see Mezger, Mathis, and Panagia 1982, hereafter MMP, for a summary of observational and experimental

determinations of $K(\lambda)$). Given the value of n, the dust temperature and other related physical quantities can be estimated directly from the observations.

(iv) Dust temperature profile

The dust temperature profile in the galactic plane is shown in Figure 5(a), and is derived from the ratio of observed intensities at 150 and 250 μm. The temperature profile shows no significant trends over the 10°-45° longitude range, and is essentially constant over this range with a mean value of 23 K, very similar to the average value of 25 K found by Ryter and Puget (1977) from their analysis of the FIR emission of nine molecular clouds.

(v) Optical depth and column density profiles

For an optically thin source, the optical depth of the dust in a given band is

$$\tau(\lambda) = \frac{I_{obs}}{B(\lambda,T)\ \Delta\lambda} \qquad (1)$$

where I_{obs} is the observed intensity in the band, $B(\lambda,T)$ is the Planck function at the effective wavelength λ of the band and at dust temperature T, and $\Delta\lambda$ is the effective bandwidth. The optical depth profile in the galactic plane at the effective

wavelength of 250 μm of band 2 is shown in Figure 5(b). The results show that the Galaxy is optically thin at the FIR/SMM wavelengths. The mean opacity at 250 μm in the 10^{o} - 45^{o} longitude interval is 6×10^{-3}, and the maximum observed value in the band is about 10^{-2}. Comparison of the optical depth and temperature profiles illustrates that the large variations observed in SMM emission are primarily due to changes in dust column density, rather than variations in the temperature of the emitting dust.

The optical depth profile can be converted to a dust mass column density profile using the relation

$$M_d = \tau(\lambda)/K(\lambda) \qquad (2)$$

where $K(\lambda)$ is the mass absorption coefficient (in cm^2/g) of the dust at wavelength λ. Summaries of observational and experimental data related to the optical properties of the dust are presented by Draine (1981) and MMP. For the present analysis, a value of $K=4.6$ cm^2/g at $\lambda=300$ μm has been adopted, which is about equal to the mass absorption coefficient of uncoated lunar silicate type spheres (Aanestad 1975) and amorphous silicates (Day 1981). As stated above, a spectral index of $n=2$ has also been assumed. The derived dust mass column density profile (in g/cm^2) is identical to the optical depth profile at 250 μm scaled by a multiplicative factor of 0.15.

(vi) Total infrared surface brightness profile

The far infrared brightness I_{FIR}, integrated over all wavelengths, can be estimated from the observed intensity at 150 μm if the fraction of the total energy observed in the band is known. At the characteristic temperature of 23 K, this fraction is approximately 40 percent of the total flux emitted for a spectral index n=2. The longitudinal profile of I_{FIR} (averaged over $|b| \leq 0.5^{\circ}$) is shown in Figure 5c. The mean value in the range, $\ell = 10^{\circ}-45^{\circ}$, is 9×10^{-5} W $m^{-2}sr^{-1}$. The FIR brightness shown in the figure is quite insensitive to the particular dust model adopted in this paper. It increases by only 20 percent if a spectral index of n=1.5 is assumed, and changes by only 5 percent if the multicomponent dust model of MMP (given in Table 4) is adopted. This fact, and the appreciably lower brightness of the emission from the galactic plane at shorter wavelengths reported by Price (1981) and Hayakawa et al. (1979) indicate that the FIR/SMM emission in the spectral range of this survey dominates the total infrared luminosity from the galactic plane.

The value of the quantities derived thus far, averaged over the $\ell = 10-45^{\circ}$ and $|b| \leq 0.5^{\circ}$ region of the galactic plane, are summarized in Table 2. These quantities depend only on our measurements and the assumed optical properties of the dust.

Further discussion of the diffuse emission is given in section IV, where the FIR/SMM observations are compared with observations of ^{12}CO in the galactic plane.

b) The Compact Sources

A list of 80 prominent compact sources found in the survey data is presented in Table 3. All compact sources reported here were identified by demanding spatial coincidence of local maxima in the 150 and 250 μm maps of the survey. Local maxima within 12 arcminutes of each other in the different bands were assumed to be the same source. When a local maximum was also found in the longest wavelength band within 15 arcminutes of a source, its 300 μm flux is included in the table. This procedure preferentially selects compact sources and discriminates against extended features as well as the extended emission from the galactic plane itself.

Table 3 also includes various source properties derived assuming a single temperature dust emission model. This is an obvious simplification of the physical condition in the sources, since many are associated with known HII regions and are probably centrally heated. A comparison of our survey data with those from a similar survey at shorter wavelengths reveals a complex dust-temperature distribution around several prominent sources.

The results of this comparison are presented elsewhere (Campbell et al. 1984).

For weak sources embedded in regions of high diffuse emission, even the peak flux density presented here may be significantly contaminated by the underlying diffuse background. No attempt has been made to subtract this background emission. The derived physical conditions in these sources may therefore be more representative of the diffuse emission region than of the individual compact source.

Finally, Table 3 indicates whether the sources have been observed previously at other FIR wavelengths, in the radio continuum, or in the J=1-0 line of the CO molecule. For the CO and radio identifications, sources were considered to be the same if they were spatially coincident within $\sim$ 18 arcminutes. For the FIR identification the spatial coincidence requirement was relaxed to be consistent with the estimated positional uncertainty of the various balloon experiments.

Most of the sources reported in this paper are seen to be associated with strong 5 GHz radio continuum emission peaks (Altenhoff et al. 1970). These radio continuum sources are all typical of thermal emission sources. Some of the FIR emission

peaks which are not identified with a region of strong radio continuum emission are located near fairly strong molecular line emission regions (Cohen et al. 1980). These sources are either not associated with ionized gas, or the ionized gas is too diffuse to be detected as a compact radio source. About half the sources reported here have not been previously detected at FIR or SMM wavelengths.

IV. COMPARISON WITH OTHER SURVEYS OF THE GALACTIC PLANE

a) Comparison With CO Distribution

We have compared the distribution of the infrared emission observed in the FIR/SMM survey with the distribution of molecular gas in the Galaxy inferred from the Goddard Institute of Space Studies (GISS) extended CO survey results of Cohen et al. (1980). These ^{12}CO survey observations were made with a 7.5 arcmin beam, making direct comparison with these FIR/SMM survey observations appropriate.

The longitudinal profile of the ^{12}CO intensity in the galactic plane is shown in Figure 6a. The profile represents the velocity-integrated ^{12}CO intensity averaged, as were our survey data, over the latitude range $|b| \leq 0.5^{o}$. The integrated ^{12}CO intensity can be converted to a hydrogen column density N_H ($= N(HI)+2N(H_2)$), using the calibration:

$$N_H\ (cm^{-2}) = 3.2 \times 10^{20} \int T(^{12}CO)\ dv\ (K\ km\ sec^{-1}) \qquad (3)$$

(Solomon, Scoville, and Sanders 1979; Savage and Mathis 1979; Dickman 1978). This calibration is consistent with more recent estimates of the average extinction-to-^{13}CO column density measurements (Frerking, Langer, and Wilson 1982), and is also well within the calibration range calculated by Lebrun et al. (1983) from the comparison of the GISS CO survey and the COS-B gamma-ray survey of the galactic plane. The use of a constant calibration factor over a large range of galactic longitudes may give rise to errors resulting from the presence of metallicity gradients in the Galaxy. However, observations of large scale metallicity gradients within the Galaxy, summarized by Pagel and Edmunds (1981), show no significant gradients in the disk for $\ell^{II} > 20^{\circ}$. The effects of metallicity gradients on the results of our analysis of the 10°-45° region of the plane are therefore expected to be small. In the following, we derive the dust-to-gas mass ratio and the total infrared luminosity per unit hydrogen mass, as inferred from comparison of the dust distribution with the results of the ^{12}CO survey.

(i) Dust-to-gas mass ratio

The dust-to-gas mass ratio, Z_d, is given by

$$Z_d = 4.30 \times 10^{23}\ M_d/N_H, \qquad (4)$$

which is inversely proportional to the mass absorption

coefficient of the dust. The value of Z_d therefore depends on the assumed dust model. For the value of K(300 μm) adopted in this paper, the average dust-to-gas mass ratio in the 10°-45° longitude range is 0.01. This value is consistent with cosmic abundance arguments (e.g. Cameron 1973) and implies that virtually all of the available condensable material is required to be in grains to produce the observed radiation. Models for the origin of the FIR/SMM wavelength emission in which only a fraction of the available dust gives rise to the observed emission (such as that proposed by MMP, as discussed in section VI), require a correspondingly higher value for K(300 μm). For clarity, we have plotted the longitudinal profile of the inverse ratio, i.e. the gas-to-dust mass ratio, in the galactic plane in Figure 6b. The profile shows very little dispersion at the resolution of these surveys (rms variations are only 25% of the mean). The mean value of Z_d is relatively constant over the range of longitudes discussed here, and is the same as the average value determined in a $1^{\circ}x2^{\circ}$ field of view around the galactic center (Stier et al. 1982) from a comparison with ^{13}CO observations of the galactic center region (Heiligman 1981). This constancy does not, however, exclude the existence of metallicity gradients towards the galactic center since both the CO and the dust could follow the metallicity trends in the Galaxy.

(ii) The mean infrared luminosity per unit mass

An important astrophysical quantity is the infrared luminosity per unit mass of hydrogen, L_{IR}^{H}, given by

$$L_{IR}^{H} = 4\pi\ I_{FIR}/N_H\ . \qquad (5)$$

The profile of L_{IR}^{H} in the galactic plane, shown in Figure 6c, has a mean value of 8 $L_\odot/M_\odot$, equivalent to 2.5×10^{-30} W/H-atom. The profile shows significant variations with galactic longitude, implying variations in the mean radiative energy density along the galactic plane. The average value of L_{IR}^{H} is more than an order of magnitude larger than that which would arise from dust heated primarily by a stellar radiation field comparable to that in the solar neighborhood. The mean specific luminosity is very close to the mean value of 6 $L_\odot/M_\odot$ found by Ryter and Puget (1977) in a study of nine individual molecular clouds. In deriving this value, they used the same calibration as that given in equation (3) to convert CO intensities to H column densities. The similarity in these specific luminosity values over a large portion of the galactic plane seems to offer at least circumstantial evidence for the association of the FIR/SMM emission with dust in molecular clouds. This topic is addressed in more detail in section VI below.

b) Comparison With 5 GHz Survey of the Galactic Plane

It has been argued (Mezger 1978) that a significant fraction of the volume of the Galaxy is filled with an extended, low density (ELD) ionized gas heated by OB stars. Furthermore, Mezger, Mathis, and Panagia (1982) have argued that most of the far infrared emission from the Galaxy arises from dust that resides in these ELD HII regions.

Gispert, Puget, and Serra (1982) constructed a longitudinal profile of the 5 GHz continuum emission integrated over the $\pm 1^{\circ}$ latitude interval from the 11 arcmin survey of the galactic plane of Altenhoff et al. (1970). The profile shows the emission from compact radio sources superimposed on a diffuse component. An upper limit on the integrated continuum free-free emission from ELD HII regions in the $10\text{-}45^{\circ}$ longtiude interval is $\sim 2\times10^{4}$ Jy rad^{-1}. The flux of Lyman continuum (Lyc) photons required to sustain the ionization of this diffuse gas is given by (e.g. Mezger, Smith, and Churchwell 1974)

$$N_{Lyc}\ (cm^{-2}\ s^{-1}) = 817\ S_{5GHz}\ (Jy), \qquad (6)$$

where we have adopted an electron temperature of 8000 K in the HII region. An upper limit on L(Lyα), the Lyman α luminosity from the ionized gas, can be obtained by assuming that each Lyc photon is absorbed by the gas and re-emitted as a Lyα photon. A quantity that measures the importance of these photons in

heating the dust is the infrared excess (IRE) ratio defined by Mezger, Smith, and Churchwell (1974) as

$$IRE = L_{IR}/L(Ly\alpha), \qquad (7)$$

where L_{IR} is the total infrared luminosity. The average infrared flux (integrated over the same latitude range as the 5 GHz flux) in the 10-45° longitude interval is 2.3×10^{-6} W m^{-2} rad^{-1}, giving, in conjunction with the Lyα flux ($= N_{Lyc} x h\nu_{Ly\alpha}$), a lower limit of 9 for the average value of the IRE ratio in that longitude interval.

We constructed models of dusty HII regions created by ZAMS stars of various spectral type embedded in a medium of uniform density. Stellar parameters were taken from Panagia (1973), and the computational procedure was similar to that used by Panagia (1974). We first calculated the IRE ratios for stars embedded in a low density medium of 5 cm^{-3}, typical of ELD HII regions. The fraction of stellar radiation that is directly absorbed by the dust inside the Stromgren sphere of an O4 star is only 0.12, and declines rapidly for later type stars. The value of the IRE ratio is therefore very sensitive to the fraction, f_{abs}, of non-ionizing and nebular radiation that is absorbed in the adjacent/overlapping Stromgren spheres that constitute the galactic ELD ionized gas. From Mezger (1978) we estimate $f_{abs} = 0.70$, which gives an IRE value of less than 7 for a cluster of

stars with an initial mass function (IMF) given by Miller and Scalo (1979). Larger IRE ratios can be attained if the cluster of stars is embedded in a higher density medium, where the dust inside a given Stromgren sphere competes more effectively for the Lyc photons. IRE ratios significantly higher than 9 can also be achieved by adopting a lower value ($<45M_{\odot}$) for the high-mass cutoff, or equivalently by postulating the existence of an excess population (over the Miller-Scalo IMF) of low mass stars in the cluster. This latter interpretation was adopted by Boissé et al. (1981) in their analysis of the IRE ratio of individual FIR/5 GHz sources.

V. ORIGIN OF THE DIFFUSE FIR/SUBMM EMISSION

The radiation detected in this and other FIR galactic surveys is generally attributed to thermal radiation from dust; however, the nature and location of the dust particles and the sources that heat them are still a matter of controversy. Two distinct models for the origin of the diffuse FIR/SMM emission have been discussed in the literature, and will be examined here.

In the first model, most of the diffuse emission arises from dust particles that are located in giant molecular clouds (GMC), heated by embedded (yet unobservable) OB and late-type stars. In this model for the FIR/SMM emission (Fazio and Stecker, 1976),

the dust and gas are thermally and dynamically coupled; i.e. the dust temperature is related by a constant factor to that of the gas, and the dust-to-gas mass ratio is taken to be a constant throughout the galactic plane. Cheung et al. (1984) adopted this model and used the small beam CO survey data of the SUNY CO survey (e.g. Sanders 1981) to determine the gas temperature and column density, and thus derive an expected longitudinal profile for the FIR/SMM wavelength dust emission. A comparison of their derived profile with our observations shows a general similarity, but significant discrepancies are apparent, suggesting some violation of their model assumptions. The constancy of the dust-to-gas mass ratio inferred from the survey supports their assumption that the dust and gas are dynamically coupled. The model shortcomings are therefore most likely related to their assumption that the gas-to-dust temperature ratio is constant. This is not surprising, since theoretical calculations (see MMP for reference) suggest that the dust and gas temperature decouple at gas density $n(H_2) < 7 \times 10^3$ cm^{-3}, whereas the average density in GMC's is only 300 cm^{-3}.

A different approach to the same model was taken by Ryter and Puget (1977), who compiled far-infrared and CO data for nine molecular clouds associated with known HII regions. From their study they derived a typical dust temperature of 25 K, and an

infrared luminosity per unit mass of hydrogen of 6 $L_{\odot}/M_{\odot}$, which, they argue, should be typical of molecular clouds and therefore of the large scale galactic emission. The astrophysical implications of these assumptions in light of the results of their recent far infrared survey of the galactic plane are discussed by Gispert, Puget, and Serra (1982).

In the second model, most of the diffuse emission arises from dust particles located in extended low density HII regions, heated by field OB stars. This model (hereafter referred to as the ELD model), originally suggested by Mezger (1978) and more recently updated by MMP, is based on the observation that OB stars spend most of their lifetime outside of their nascent clouds, ionizing ELD HII regions. In this case, most of the diffuse emission arises from the small fraction ($\sim$ 3%) of the total interstellar dust found in the ELD HII regions. This dust is heated to a typical temperature of 30 K by known OB stars. The total infrared luminosity from the galactic plane is therefore constrained by the observed luminosity of OB stars, which is about 7×10^9 $L_{\odot}$ (MMP). Most of the dust in the Galaxy resides in molecular clouds, and in the ELD model is heated only by the attenuated interstellar radiation field. This limits the bulk of the dust mass to a temperature less than 12 K, similar to that observed in nearby dark clouds (Keene 1981).

Drapatz (1979) constructed a detailed model of the Galaxy in which the dust is heated by known OB, AF, and late-type stars. The predicted FIR/SMM intensity is in good agreement with the observations, with all three groups of stars contributing about equally to the heating of the dust. The total infrared luminosity inferred from the model is $>5\times10^9$ $L_\odot$. This model therefore, in general, supports the idea that the observed FIR luminosity can be accounted for by known stars; however, given the uncertainties in the parameters of the model, a higher inferred FIR luminosity cannot be ruled out.

To what extent can the present survey discriminate among the various models for the origin of the diffuse FIR/SMM emission? In principle, observational constraints on the location and temperature distribution of the dust and the total infrared luminosity emitted from the galactic plane may distinguish between the models. In practice, any distinction is considerably complicated by the poorly known optical properties of the interstellar grains, and by the uncertainties in the mass estimates of the gas in the Galaxy. In spite of these uncertainties, we find that the results of our survey favor a model in which the dominant emission originates from dust located in giant molecular clouds (hereafter referred to as the GMC model).

a) Location of the Dust

A comparison of the dust mass column density and the ^{12}CO intensity profiles shows a strong correlation between the gas and the dust distribution, consistent with close physical association between the molecular gas and the dust responsible for the FIR/SMM emission. However, the general concentration of interstellar matter into spiral arms would tend to produce such large-scale correlation whether or not the components are physically interacting. A nearly equally good correlation should exist between the diffuse FIR/SMM emission and the diffuse radio thermal emission, although it is not apparent in the 5 GHz longitudinal profile given by Gispert, Puget, and Serra (1982), from which the major contribution of discrete sources has not been removed. Such a correlation would, however, be expected since ELD HII regions are also physically located in the vicinity of spiral arms. A simple comparison of low angular resolution intensity profiles can therefore not discriminate between the models described above.

b) Temperature Distribution of the Interstellar Dust

In the ELD model most of the mass of interstellar dust that resides in molecular clouds is only heated by the attenuated interstellar radiation field and attains a temperature of no more

than $\sim$ 12 K. Such a massive, cold dust component should be the dominant emitter at millimeter wavelengths, specifically, in the SMM/millimeter large-beam sky survey of Owens, Muehlner, and Weiss (1979; hereafter referred to as OMW). These investigators detected no emission in their low frequency band, giving a 3σ upper limit of 8×10^{-12} Wm^{-2} for the 1-3.3 mm flux. To check the consistency of the ELD model with this upper limit, we calculated the flux predicted by the model in the bands of both our own and OMW's surveys. To estimate the fluxes in the large beams (1.6°) of the latter survey, a gaussian shape with a FWHM of 0.9° was assumed for the latitudinal distribution of the emission from the galactic plane. The ELD model was represented by the various dust components summarized in Table 4. To be definitive, we adopted the dust temperature in dark globules as representative of that of the dust in molecular clouds (see Table 4). Clearly, the dust in the molecular clouds may be colder due to the larger attenuation of the interstellar radiation field (ISRF). This effect is, however, partially offset by the presence of embedded sources which increase the dust temperature above that expected from heating by the attenuated ISRF alone. We therefore do not expect the dust temperature in clouds to be significantly lower than the value used in Table 4. In that case, the spectrum of the dust is still in the Rayleigh-Jeans regime at 1 mm wavelength, and the fluxes observed in OMW's low frequency band

will scale roughly linearly with dust temperature. The results of these calculations are given in Table 5, which compares the predicted fluxes, normalized to produce the best fit to the observed fluxes in our 150 μm and 250 μm bands, to the observations of OMW. The results show that the cold GMC dust component required by the ELD model would emit a significant flux in the OMW low frequency band, about 3 times larger than their 3σ upper limit. Most of the emission is from silicate grains for which we adopted a temperature of 10 K. In a recent revision of their model, Mathis, Mezger, and Panagia (1983) calculated the temperature of the dust in molecular clouds taking the effect of embedded sources into account. The resulting silicate temperature was found to be ∿ 6 K, which somewhat reduces, but does not eliminate the discrepancy with the observations of the OMW survey. This discrepancy can be eliminated by adopting a steeply declining emissivity for the dust at FIR/SMM wavelengths with a spectral index > 3. However, the theoretical long-wavelength value of the emissivity index is 2, and it is probably smaller if impurities affect the optical properties of the dust at these wavelengths. For the sake of comparison, the flux predicted in the GMC model has also been calculated for the various bands, assuming an isothermal dust model with T=23 K. The results show that this simple model is consistent with the observations of OMW. The dust model used in these calculations

is admittedly oversimplified, and the use of a multi-component dust model which takes into account the observational constraints implied by the OMW survey is obviously more appropriate.

c) The Total Infrared Luminosity of the Galaxy

The results of our survey show that a mean luminosity per unit mass of hydrogen of 8 $L_\odot/M_\odot$ is typical for a large portion of the inner galactic plane. The importance of this specific luminosity is that it can yield an estimate of L_{IR}, the total infrared luminosity of the Galaxy, which is not dependent on detailed knowledge of the distance of the sources. Adopting a conservative estimate of 2×10^9 $M_\odot$ of hydrogen inside the solar circle (e.g. Cohen 1978), the total infrared luminosity inferred from our observations is $(1-2)\times10^{10}$ $L_\odot$. The above mass estimate is consistent with our adopted calibration for N_H/CO. Alternatively, using the calibration of $N_H=7.2\times10^{20} \int T(^{12}CO)dv$ and a total hydrogen mass of 3.6×10^9 $M_\odot$ in the inner solar circle (1.5-10 kpc regions; Sanders, Solomon, and Scoville, 1984) gives approximately the same value for L_{IR}. The major uncertainty in the value of L_{IR} results from the uncertainty in the estimate of the amount of hydrogen in the Galaxy. The hydrogen mass may be uncertain by a factor of two, and is probably higher than the estimates used in the above calculations.

The above estimates yield a total infrared luminosity larger by a factor of 3 than the luminosity available from known OB stars in the ELD model. This energy constraint supports the model in which the emission is dominated by dust located in giant molecular clouds and heated by embedded, yet unobservable, OB stars and/or nonionizing lower mass stars.

d) The Far Infrared Properties of Interstellar Grains

An important feature in the ELD model is that the diffuse FIR/SMM emission arises from only a small fraction of the interstellar dust, which is nevertheless able to produce the observed infrared brightness from the galactic plane. This is possible because MMP adopted a large value for the dust emissivity. More specifically, MMP adopted a value of 100 cm^2/g for the mass absorption coefficient of silicate grains at 300 μm, which is more than ten times greater than the value suggested by the absorptive properties of olivine and lunar silicate-type particles (Aanestad 1975, Day 1981). MMP based their value for the emissivity on laboratory infrared measurements of synthetic magnesium silicates (Day 1976). The amorphous silicates in the 1976 experiment were produced by reactions in aqueous solutions, and their optical properties are substantially different from those of subsequent vapor-produced silicates (Day 1981). The

value of K(300 μm) for the vapor-produced silicates is only ∿ 8 cm^2/g, more consistent with the value adopted in this paper. Day attributes this difference to the presence of residual water of hydration in the early gel-produced silicates which significantly boosted their far-infared absorption. The vapor-produced silicates compare favorably with astronomical silicates, as suggested by comparison of their mid-infrared (7-33 μm) extinction properties with those inferred from astronomical observations (Day 1979).

Finally, Draine and Lee (1984) recently calculated infrared absorption cross sections of silicate and graphite particles using available laboratory and astronomical data. Their value for K(300 μm) is ∿ 4 cm^2/gr for the silicates and ∿ 10 cm^2/gr for the graphite, in good agreement with our adopted value. A significantly higher value for K in the FIR would, according to their calculations, violate the Kramers-Kronig relation between the optical constants in the various wavelength regimes.

VI. SUMMARY

The initial results of our large scale FIR/SMM survey of the first quadrant of the galactic plane show that the observed emission arises from both compact sources and an underlying diffuse background which accounts for the bulk of the emission within $|b| \leq 1^{\circ}$ of the plane. A list of the compact sources, their derived characteristics, and their association with known peaks of 5 GHz or CO emission is given in Table 3. The derived characteristics of the diffuse background averaged over the $10-45^{\circ}$ longitude interval are given in Table 2.

Comparison of the distribution of the infrared emission detected in our survey with the Cohen et al. (1980) CO survey of the galactic plane shows that, if the optical properties of the dust are similar to those of vapor-produced silicates, then nearly all of the available condensable material is required to produce the emission. The total infrared luminosity inferred from the comparison is $1-2 \times 10^{10}$ $L_{\odot}$, higher than that available from visible OB stars alone in the Galaxy.

Comparison with the Altenhoff et al. (1970) 5 GHz survey of the galactic plane shows that the infrared excess ratio (IRE) of the diffuse emission component is $\gtrsim 9$. This value is larger than that expected from dust inside ELD HII regions, suggesting that

the heating sources of the dust are embedded in higher density molecular clouds. IRE ratios significantly larger than 9 may require the existence of an excess population (compared with the Miller-Scalo IMF) of low-mass stars that contribute to the heating of the dust.

All of the above analysis suggests that the FIR/SMM emission detected in this survey arises predominantly from dust that is associated with molecular gas, rather than from dust that is embedded in extended low-density ionized regions in the Galaxy.

ACKNOWLEDGEMENTS

We thank the many engineers and technicians at the Goddard Space Flight Center who contributed so substantially to the development and testing of this payload. The staff of the National Scientific Balloon Facility in Palestine, Texas provided cheerful, patient, and competent assistance in the launch and recovery of the survey instrument in flights 1184P, 1209P, and 1301P. We acknowledge helpful suggestions from S. Drapatz and J. L. Puget. We thank Phyllis Bayne for her skillful typing of this manuscript. This work was supported by NASA RTOP 188-41-55.

TABLE 1: SUBMILLIMETER SURVEY INSTRUMENT PARAMETERS

TELESCOPE CONFIGURATION:

Optics	Cassegrain
Primary mirror diameter	1.2 meter
Primary focal ratio	f/0.37
Effective focal ratio	f/4
Chopper frequency	10 Hz square wave
Beam separation	20 arcmin
Field-of-View	10 x 10 arcmin
Scan Rate	20 arcmin s^{-1}

FILTER PHOTOMETER:	Band 1	Band 2 (Flight 1)	Band 2' (Flight 2)	Band 3
Effective wavelength[a]	150 μm	250 μm	190 μm	300 μm
Cut-on wavelength (50%)	112 μm	225 μm	150 μm	265 μm
Effective bandwidth (Hz)[a]	1.2×10^{12}	6.0×10^{11}	9.1×10^{11}	5.0×10^{11}
NER (W $cm^{-2}sr^{-1}Hz^{-1/2}$)	5.0×10^{-11}	1.9×10^{-11}	3.1×10^{-11}	1.1×10^{-11}
NEFD (Jy $Hz^{1/2}$)	350	270	290	190

[a] Computed assuming a T = 25 K source, λ^{-2} dependent emissivity law.

TABLE 2: DERIVED PHYSICAL CONDITIONS IN THE INNER GALAXY

QUANTITY	UNITS[a]	AVERAGE VALUE[b]
Dust temperature[c]	T_d (^oK)	23 ± 1.4
Dust optical depth	τ_d (250 μm)	$(6.2 \pm 2) \times 10^{-3}$
FIR brightness	I_{FIR} ($W\ m^{-2}\ sr^{-1}$)	$(8.8 \pm 2) \times 10^{-5}$
Dust-to-gas mass ratio[d]	Z_d	0.01
IR luminosity per H mass	L_{IR}^{H} ($L_\odot/M_\odot$)	8.2 ± 2
IR excess ratio	IRE	≥ 9
Thickness, diffuse emission	b^{II}(FWHM)	$\sim 0.9^\circ$

[a] Symbols are explained in text.

[b] Quantities averaged over the galactic longitude interval $\ell^{II} = 10^\circ - 45^\circ$. Errors quoted are the rms dispersion about the mean value.

[c] Calculated from the 150 μm to 250 μm flux ratio, and assuming an emissivity index n = 2.

[d] Calculated for a mass absorption coefficient K(300 μm) = 4.6 $cm^2 g^{-1}$.

TABLE 3: COMPACT SOURCES - SUBMILLIMETER SURVEY OF THE GALACTIC PLANE[a]

Source No.	Position (1950.0) Galactic Coordinates	R.A.	DEC.	Peak Flux Density (10^3 Jansky) Band 1	Band 2	Band 2'	Band 3	Dust Temp. (K)	Optical Depth (10^{-3})	Dust Column Density (10^{-4} g/cm^2)	Flight No.	Detected in Other Surveys: 5 GHz	CO	Far IR
	(1)	(2)	(3)	(4)	(5)	(6)	(7)	(8)	(9)	(10)	(11)	(12)	(13)	(14)
1	355.6-0.2	$17^h32^m20^s$	$-32^\circ44'$	35.		26.	9.2	25	4.4	9.2	2	1	-1	
2	356.3-0.1	17 33 40	-32 05	31.		22.	6.6	28	2.4	4.9	2	0	-1	
3	356.8+0.1	17 34 10	-31 34	31.		21.	6.5	28	2.3	4.7	2	2	-1	H
4	359.5-0.3	17 42 20	-29 29	169.		108.	33.	30	11.	22.	2	1	-1	H
5	359.9-0.3	17 43 20	-29 09	224.		137.	43.	30	14.	28.	2	1	-1	H,G,N
6	0.5-0.2	17 44 20	-28 35	339.		203.	76.	27	30.	61.	2	1	-1	H,G,N
7	5.9-0.3	17 57 10	-24 00	40.		24.	6.5	34	1.7	3.3	2	1	-1	H,E,G,N
8	6.9-0.1	17 58 30	-23 02	28		21.	9.7	21	6.6	14.	2	1	-1	N
9	8.3+0.0	18 01 10	-21 46	24.		17.	7.1	23	4.0	8.5	2	1	-1	H
10	10.3-0.3	18 6 30	-20 10	57.	28.	33.	14.	25	6.6	14.	*	1	-1	H,E,G
11	10.6-0.3	18 7 10	-19 55	48.	25.		16.	21	11.	24.	1	1	-1	N
12	11.5-0.3	18 9 0	-19 08	23.	12.		9.6	19	8.3	19.	1	2	0	
13	11.9-0.2	18 9 30	-18 44	27.	13.		4.4	33	1.2	2.3	1	2	1	
14	12.9-0.2	18 11 30	-17 51	73.	30.	47.	15.	30	5.3	11.	*	1	1	H,N
15	13.3 0.0	18 11 30	-17 24	38.	20.	27.	9.6	26	4.6	9.7	*	1	1	
16	13.6-0.2	18 12 50	-17 17	36.	20.	24.	12.	22	6.9	15.	*	2	2	
17	13.9-0.1	18 13 10	-16 56	37.	18.	25.	11.	22	6.7	14.	*	0	1	
18	14.3-0.5	18 15 30	-16 46	31.		21.	7.9	25	3.6	7.5	2	2	0	
19	14.5 0.0	18 14 00	-16 21	41.		27.	11.	25	4.9	10.	2	1	1	H
20	15.0-0.7	18 17 30	-16 15	130.	44.	76.	26.	30	8.4	17.	*	1	1	H,G,E,N
21	15.2-0.1	18 15 40	-15 47	29.		19.	5.0	32	1.4	2.8	2	0	1	H
22	16.4-0.2	18 18 30	-14 47	33.	13.	25.	7.3	28	2.9	6.1	*	1	1	G
23	17.0-0.1	18 19 10	-14 15	27.	12.	22.	8.3	23	5.0	11.	*	2	1	N
24	17.1+0.9	18 15 50	-13 41	27.	11.	19.	7.7	24	4.0	8.4	*	1	1	N,G
25	17.6+0.2	18 19 20	-13 32	19.	8.9	12.	4.4	28	2.0	4.2	*	2	1	
26	17.7+0.6	18 18 10	-13 15	16.	8.6						1	0	1	

	(1)	(2)	(3)	(4)	(5)	(6)	(7)	(8)	(9)	(10)	(11)	(12)	(13)	(14)
27	18.1+2.0	18 13 50	-12 14	15.	4.3	9.6					*	1	-1	
28	18.2-0.3	18 22 20	-13 14	38.	15.		8.2	28	3.0	6.3	1	1	1	G
29	18.7-0.1	18 22 40	-12 42	29.	12.		9.5	22	5.9	13.	1	0	1	N
30	19.0-0.1	18 23 10	-12 26	42.	19.		10.	26	4.3	9.0	1	1	1	N
31	19.4+0.0	18 23 40	-12 02	34.	18.		8.6	25	3.9	8.2	1	2	1	
32	19.7-0.2	18 24 50	-11 52	39.	15.		8.9	27	3.6	7.4	1	1	1	
33	19.8-0.8	18 27 10	-12 04	20.	9.7		4.0	30	1.3	2.6	1	2	0	
34	20.6-0.3	18 27 00	-11 07	31.	13.		7.2	27	2.9	6.1	1	1	1	N
35	21.3-0.3	18 28 20	-10 30	26.	14.		9.7	20	7.0	15.	1	0	0	
36	22.3-0.2	18 29 50	-9 34	30.	15.		10.	21	6.4	14.	1	2	1	N
37	22.9-0.3	18 31 20	-9 05	44.	19.		11.	25	4.9	10.	1	1	1	N,G
38	23.3-0.2	18 31 40	-8 41	63.	29.		20.	22	11.	25.	1	1	1	N
39	23.9+0.1	18 31 50	-8 01	40.	19.		11.	24	5.3	11.	1	2	1	
40	24.4+0.1	18 32 40	-7 34	46.	22.		14.	23	7.8	17.	1	1	1	N
41	24.8+0.1	18 33 30	-7 13	52.	19.		11.	28	3.9	8.1	1	1	1	G?
42	25.4-0.2	18 35 40	-6 50	44.	17.		9.0	29	3.2	6.6	1	1	1	N
43	25.7-0.1	18 35 50	-6 31	37.	17.		12.	22	7.2	15.	1	1	0	
44	26.2+0.0	18 36 30	-6 02	35.	15.		10.	23	5.8	13.	1	1	1	
45	26.6+0.1	18 36 50	-5 37	31.	14.		7.8	25	3.5	7.3	1	1	1	
46	27.2+0.0	18 38 20	-5 08	28.	12.		7.2	25	3.3	6.9	1	1	1	
47	28.3+0.0	18 40 20	-4 10	37.	18.		12.	22	7.5	16.	1	0	1	
48	28.6+0.0	18 40 50	-3 54	36.	17.		10.	23	5.5	12.	1	1	1	G
49	28.8+3.4	18 29 10	-2 09	22.	9.2						1	1	-1	G
50	29.3-0.1	18 42 30	-3 19	28.	15.		9.6	21	6.3	14.	1	2	1	
51	29.8-0.1	18 43 30	-2 53	62.	23.		15.	25	6.8	14.	1	1	1	H,N
52	30.6-0.2	18 45 20	-2 13	101.	38.		26.	25	12.	26.	1	1	1	H,N
53	31.9+0.0	18 47 00	+0 58	17.	8.5		5.9	21	4.0	8.7	1	1	1	
54	32.7+0.2	18 47 40	+0 10	18.	7.9		6.1	21	4.0	8.8	1	2	1	
55	33.4+0.0	18 49 40	+0 21	27.	14.		7.7	24	4.0	8.5	1	1	1	N
56	34.2+0.2	18 50 30	+1 09	55.	27.		17.	23	9.6	21.	1	1	1	N,G
57	34.5+0.1	18 51 20	+1 22	27.	14.		9.8	20	7.2	16.	1	1	1	
58	35.3-1.6	18 59 00	+1 18	14.	7.6		3.0	28	1.1	2.4	1	1	-1	
59	35.5+0.1	18 53 10	+2 15	25.	11.		8.1	22	5.0	11.	1	1	1	
60	36.5+0.0	18 55 30	+3 06	17.	7.7		4.7	24	2.5	5.2	1	2	1	

	(1)	(2)	(3)	(4)	(5)	(6)	(7)	(8)	(9)	(10)	(11)	(12)	(13)	(14)
61	37.5+0.1	18 57 00	+4 02	26.	13.		6.6	25	3.0	6.2	1	1	2	
62	37.7-0.3	18 58 40	+4 01	28.	11.		7.1	25	3.3	7.0	1	1	1	N
63	38.2-0.2	18 59 20	+4 31	24.	10.		7.7	22	4.8	10.	1	0	0	
64	38.8-0.3	19 00 50	+5 00	18.	9.8		7.3	19	5.9	13.	1	0	1	G
65	39.6-0.3	19 02 20	+5 43	15.	5.9		5.2	21	3.6	8.0	1	0	0	
66	40.4+2.5	18 53 40	+7 43	10.	6.4		4.5	18	4.1	9.3	1	1	-1	
67	41.0-0.2	19 04 30	+7 00	18.	13.		3.5	30	1.2	2.4	1	1	1	N
68	42.1-0.1	19 06 10	+8 01	17.	9.4		8.2	18	8.1	19.	1	2	0	
69	42.4-0.2	19 07 10	+8 14	20.	9.0		7.1	21	5.0	11.	1	1	1	N,G
70	43.2+0.0	19 08 00	+9 02	47.	24.		12.	25	5.9	12.	1	1	1	H,G
71	44.3+0.1	19 09 40	+10 03	14.	6.7		6.5	18	6.5	15.	1	2	0	
72	45.5+0.1	19 12 00	+11 07	18.	9.3		5.0	24	2.6	5.5	1	1	1	G
73	48.8+0.1	19 18 20	+14 02	21.	7.8		5.6	24	2.7	5.8	1	1	1	
74	49.6-0.3	19 21 20	+14 33	92.	29.		19.	29	6.6	14.	1	1	0	H,G
75	50.8+0.2	19 21 50	+15 50	8.1	4.4		2.9	21	2.0	4.4	1	0	0	G?
76	51.3+0.0	19 23 40	+16 11	8.3	4.4						1	1	0	
77	53.1+0.0	19 27 10	+17 45	9.6	5.1		4.2	19	3.9	8.8	1	2	1	
78	53.6+0.0	19 28 20	+18 12	12.	8.2		6.5	17	7.8	18.	1	2	1	
79	54.1+0.0	19 29 20	+18 38	10.	6.9		4.0	20	3.2	7.1	1	2	1	
80	59.8-0.2	19 42 10	+23 29	9.7	4.1						1	2	0	G

[a] All quantities represent the average value in our beam centered on the source. Dust temperatures are calculated assuming a λ^{-2} emissivity law, from the Band 1 to Band 3 flux ratio. Band definitions are given in Table 1.

* Sources detected in both flights.

5 GHz - Coincidence with the Altenhoff *et al.* (1970) survey.

0 = No 5 GHz source apparent within $\sim 0.3^{\circ}$ of the FIR source

1 = 5 GHz source coincides with FIR peak ($\sim 0.3^{\circ}$)

2 = No 5 GHz sources, but 1.4 and/or 2.7 GHz source present in the Altenhoff survey

CO - Comparison to the GISS CO survey (Cohen *et al.*, 1980)

-1 = CO survey did not cover this region

0 = No CO peak was found within $\sim 0.3^{\circ}$ of the FIR source

1 = CO peak coincides with FIR peak ($\sim 0.3^{\circ}$)

2 = No clear CO peak identified, but FIR peak is in a complex region of significant intensity in the CO map

FAR IR - Other far infrared surveys

H = Hoffmann, Frederick, and Emery (1971)

G = Gispert, Puget, and Serra (1982)

N = Nishimura, Low, and Kurtz (1980)

E = Emerson, Jennings, and Moorwood (1973)

TABLE 4

PHYSICAL CHARACTERISTICS OF THE THREE MAIN DUST COMPONENTS IN THE ELD MODEL[a]

Association	M_{gas} ($M_\odot$)	T(graphite) ($^\circ$K)	T(silicates) ($^\circ$K)	L_{IR} ($L_\odot$)
1) Extended low density (ELD) HII regions	$\sim 1\times10^{7}$	40	27	5.2×10^{9}
2) Diffuse hydrogen	1.1×10^{9}	21	12	1.8×10^{9}
3) Molecular gas	1.2×10^{9}	14	10	3.4×10^{8}

[a] Based on Table 4 in MMP with K(300 μm) = 3.8(100) cm^2/g for graphite (silicates), and a dust emissivity index of n=2.

TABLE 5

COMPARISON OF PREDICTED FLUXES WITH LARGE BEAM OBSERVATIONS OF THE GALACTIC PLANE[a]

SPECTRAL BAND	0.4 - 1 mm (10^{-12} W m^{-2})	1 - 3.3 mm (10^{-12} W m^{-2})
MODELS[b]		
1) ELD model[c]	600	20[e]
2) GMC model[d]	300	6[e]
OBSERVATIONS	600	< 8 (3σ)

[a] Owens, Muehlner, and Weiss (1979; OMW).

[b] Model nomenclature defined in section V.

[c] Fluxes were calculated using silicate and graphite mass absorption coefficients K(λ) of 100 and 3.8 cm^2/g respectively at 300 μm, and normalized to the observations in the 150 μm and 250 μm channels of the present survey.

[d] Represented by an isothermal dust model with K(300 μm) = 4.6 cm^2/g and T = 23 K.

[e] The major uncertainty in the calculations results from uncertainty in the calibration of the frequency scale of the filters (OMW; Figure 3) which is at most 0.5 cm^{-1} (Weiss, private comm.). This uncertainty results in $\lesssim$20 percent change in the predicted flux in the 1-3.3 mm band of OMW.

REFERENCES

Aanestad, P.A. 1975, Ap. J., 200, 30.

Altenhoff, W.J., Downes, D., Goad, L., Maxwell, A., and Reinhart, R. 1970, Astr. Ap. Suppl., 1, 319.

Andriesse, C.D. 1974, Astr. Ap., 37, 257.

Boissé, P., Gispert, R., Coron, N., Wijnbergen, J.J., Serra, G., Ryter, C., and Puget, J.L. 1981, Astr. Ap., 94, 265.

Campbell, M.F., Silverberg, R.F., Hoffmann, W.F., Hauser, M.G., Niles, D.W., Stier, M., Thronson, H.A., and Kelsall, T. 1984, submitted to Ap. J.

Cameron, A.G.W. 1973, Sp. Sci. Rev., 15, 121.

Cheung, L.H. 1980, Ph.D. dissertation, Univ. of MD (NASA TM 82056).

Cheung, L.H., Fazio, G.G., Stecker, F.W., Sanders, D.B., and Solomon, P.M., 1984 (preprint).

Cohen, R.S., Cong, H., Dame, T.M., and Thaddeus, P. 1980, Ap. J. (Letters), 239, L53.

Cohen, R.S. 1978, Ph.D dissertation, Columbia Univ. (NASA TM 78071).

Day, K.L. 1976, Ap.J., 210, 614.

Day, K.L. 1979, Ap.J., 234, 158.

Day, K.L. 1981, Ap.J., 246, 110.

Dickman, R.L. 1978, Ap. J. Supp. 37, 407.

Draine, B.T. 1981, Ap. J., 245, 880.

Draine, B.T., and Lee, H.M. 1984, submitted to the Ap. J.

Drapatz, S. 1979, Astr. Ap., 75, 26.

Emerson, J.P., Jennings, R.E., and Moorwood, A.F.M. 1973, Ap. J., 184, 401.

Fazio, G.G., and Stecker, F.W. 1976, AP. J. (Letters), 207, L49.

Frerking, M.A., Langer, W.D., and Wilson, R.W. 1982, Ap. J., 262, 590.

Gezari, D.Y. 1982, Ap. J. (Letters), 259, L29.

Gispert, R., Puget, J.L., and Serra, G. 1982, Astr. Ap., 106, 293.

Hauser M. G., Dwek, E., Gezari, D., Silverberg, R., Kelsall, T., and Stier, M., 1983, Kinematics, Dynamics and Structure of the Milky Way, Shuter (ed.), p.183.

Hayakawa, S., Matsumoto, T. Murakomi, H., Uyama, K., Yamagami, T., and Thomas, J.A., 1979, Nature, 279, 510.

Heiligman, G.M. 1981, in "The Phases of the Interstellar Medium", Proceedings of a Workshop at the NRAO, ed. J.M. Dickey.

Hoffmann, W.F., Frederick, C.L., and Emery, R.J. 1971, Ap. J. (Letters), 170, L89.

Keene, J. 1981, Ap. J., 245, 115.

Lebrun, F. et al. 1983, Ap.J., 274, 231.

Low, F.J., Kurtz, R.F., Poteet, W.M., and Nishimura, T. 1977, Ap. J., 214, L115.

Maihara, T., Oda, N., and Okuda, A. 1979, Ap. J. (Letters), 227, L129.

Maihara, T., Oda, N., Shibai, H., and Okuda, H. 1981, Astr. Ap., 97, 139.

Mathis, J.S., Mezger, P.G., and Panagia, N. 1983, Astr. Ap., 128, 212.

Mezger, P.G., Mathis, J.S., and Panagia, N. 1982, Astr. Ap., 105, 372, (MMP).

Mezger, P.G. 1978, Astr. Ap., 70, 565.

Mezger, P.G., Smith, L. F., and Churchwell, E. 1974, Astr. Ap., 32, 269.

Mihalas, D., and Binney, J. 1981, Galactic Astronomy, (W.H. Freeman and Company, San Francisco).

Miller, G.M., and Scalo, J.M. 1979, Ap. J. Suppl., 41, 513.

Myers, P.C., Dame, T.M., Thaddeus, P., Silverberg, R.F., Dwek, E., and Hauser, M.G. 1984, submitted to the Ap. J.

Nishimura, T., Low, F.J., and Kurtz, R.F. 1980, Ap. J. (Letters), 239, L101.

Okuda, H. 1981, in Infrared Astronomy, IAU Symposium 96, (C.G. Wynn-Williams and D.P. Cruikshank, eds.), p. 247.

Owens, D.K., Muehlner, D.J., and Weiss, R. 1979, Ap. J., 231, 702.

Pagel, B.E.J., and Edmunds, M.G. 1981, Ann. Rev. Astr. Ap., 19, 77.

Panagia, N. 1973, A. J., 78, 929.

Panagia, N. 1974, Ap. J., 192, 221.

Price, S. D. 1981, A. J., 86, 193.

Ryter, C. E., and Puget, J. L. 1977, Ap. J., 215, 775.

Sanders, D.B., Solomon, P.M., and Scoville, N.Z. 1984, Ap. J., 276, 182.

Sanders, D.B. 1981, Ph.D. Thesis, State University of New York, Stony Brook.

Savage, B.D., and Mathis, J.S., 1979, Ann. Rev. Astron. Ap., 17, 73.

Serra, G., Puget, J.L., Ryter, C.E., and Wijnbergen, J.J. 1978, Ap. J. (Letters), 222, L21.

Serra et al. 1979, Astr. Ap., 76, 259.

Silverberg, R.F., Hauser, M.G., Mather, J.C., Gezari, D.Y., Kelsall, T., and Cheung, L.H., 1979, Proc. SPIE, 172, 149.

Silverberg, R.F. et al. 1983, Adv. Sp. Res., 3, 139.

Simon, T. 1976, A. J., 81, 135.

Solomon, P.M., Scoville, N.Z., and Sanders, D.B. 1979, Ap. J. (Letters), 232, L89.

Stier, M.T., Dwek, E., Silverberg, R.F., Hauser, M.G., Cheung, L., Kelsall, T., and Gezari, D.Y., 1982, in Proc. Caltech Workshop on the Galactic Center, Jan. 1982, D. Reidel Publishing Co., Dordrect, Holland.

Viallefond, F., Lena, P., deMuizar, M., Nicollier, C., Rouan, D., and Wijnbergen, J.T. 1980, Astr. Ap., 83, 22.

Westerhout, G. 1958, Bull. Astron. Inst. Neth., 14, 215.

Wright, E.L. 1976, Ap. J., 210, 250.

FIGURE CAPTIONS

Figure 1 - Regions of the sky (galactic coordinates) observed during the 1979 and 1980 balloon flights.

Figure 2 - Normalized transmission curves for the filters. Bands 1 and 3 were unchanged from flight 1 to flight 2. The transmission curve for band 2 is shown as a solid line for flight 1 and as a dashed line for flight 2.

Figure 3 - Contour maps of galactic plane submillimeter intensity from the first two flights. For band 1 the contours begin at 10 data numbers (DN) and increase in steps of 20 DN. For bands 2 and 3 the contours begin at 10 DN and increase in steps of 10 DN. A DN corresponds to approximately 230, 330, and 270 Jy in bands 1, 2, and 3 respectively in a 10'x10' beam. The apparent streaking of the lower contours is due to deconvolution effects. Note that in band 2 the effective wavelength of the rasters centered at about 15°, 7°, and 358° is $\lambda_{eff} = 190$ μm, since these data were obtained during flight 2 with a different filter (see Table 1 and Figure 2). Detailed maps of the galactic center region and a discussion of these sources have been presented separately (Stier et al., 1982).

Figure 4 - Galactic longitude profiles of the in-band submillimeter wavelength surface brightness I for the three survey bands, averaged over the galactic latitude range $-0.5^{\circ} \leq b \leq 0.5^{\circ}$. Note that the effective wavelength of band 2 was different in the two flights (see Table 1 and Figure 2).

Figure 5 - Longitudinal profiles of physical properties of the galactic plane as derived from the FIR/Submm surface brightness profiles: (a) Dust temperature. (b) Dust optical depth at 250 μm. (c) The FIR/Submm surface brightness. The dust mass column density (g/cm^2) profile can be obtained by multiplying by 0.15.

Figure 6 - (a) Longitudinal profile of the ^{12}CO intensity of Cohen *et al.* (1980), integrated over velocity and averaged over the latitude range of $-0.5^{\circ} \leq b \leq 0.5^{\circ}$. (b) Profile of the gas-to-dust mass ratio. (c) Profile of the far infrared luminosity per unit hydrogen mass.

Figure 1

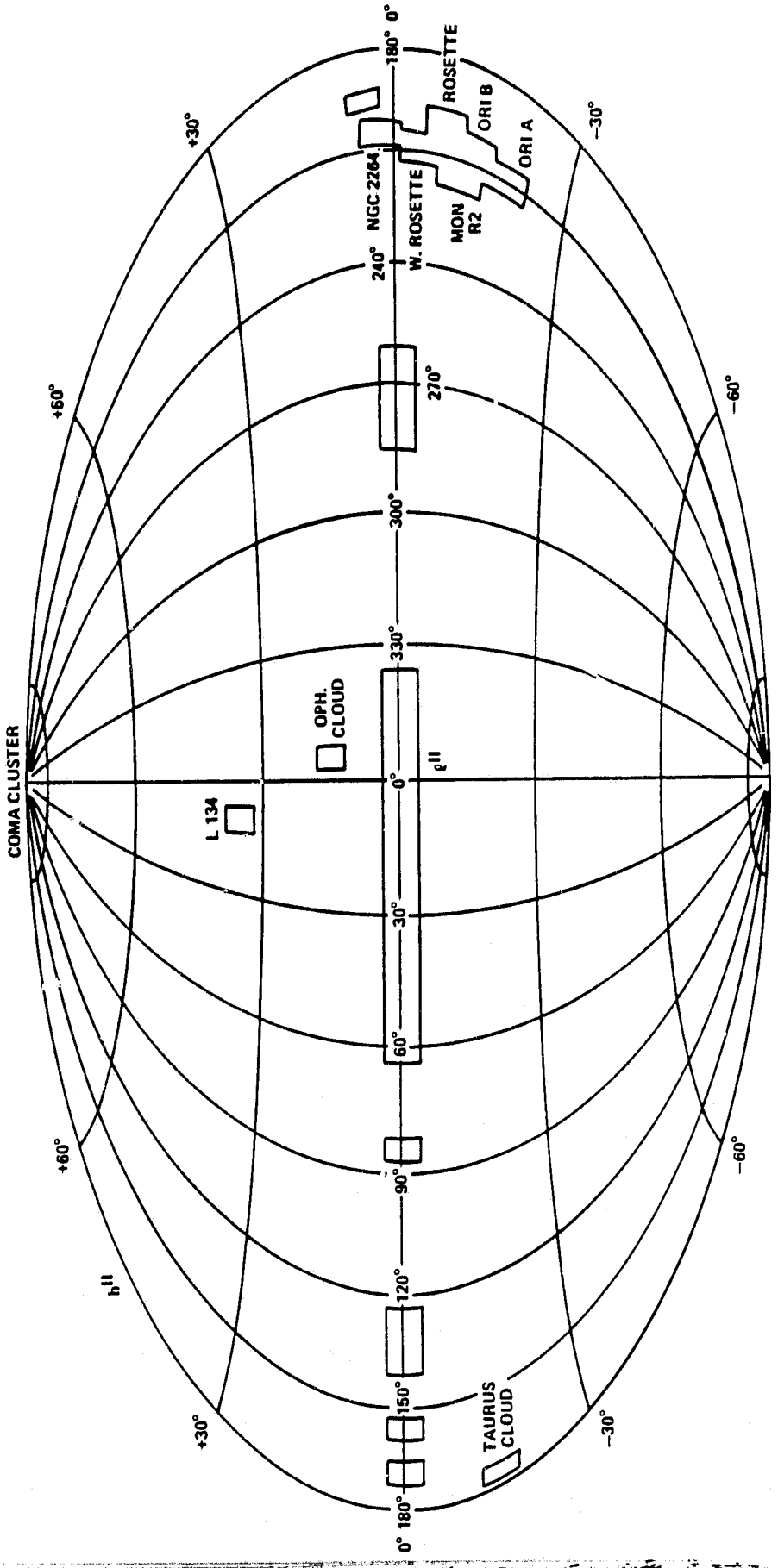

Figure 2

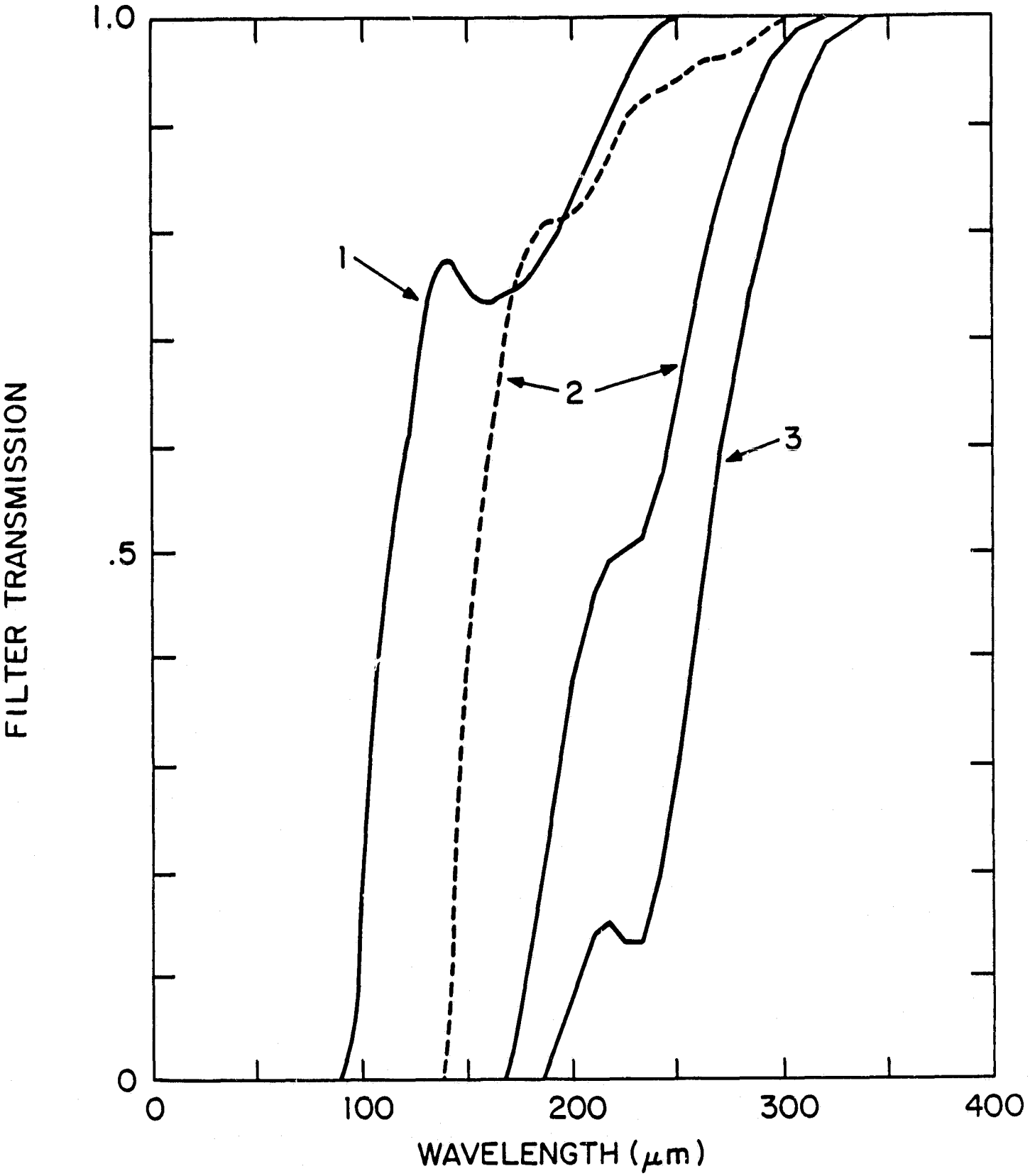

Figure 3

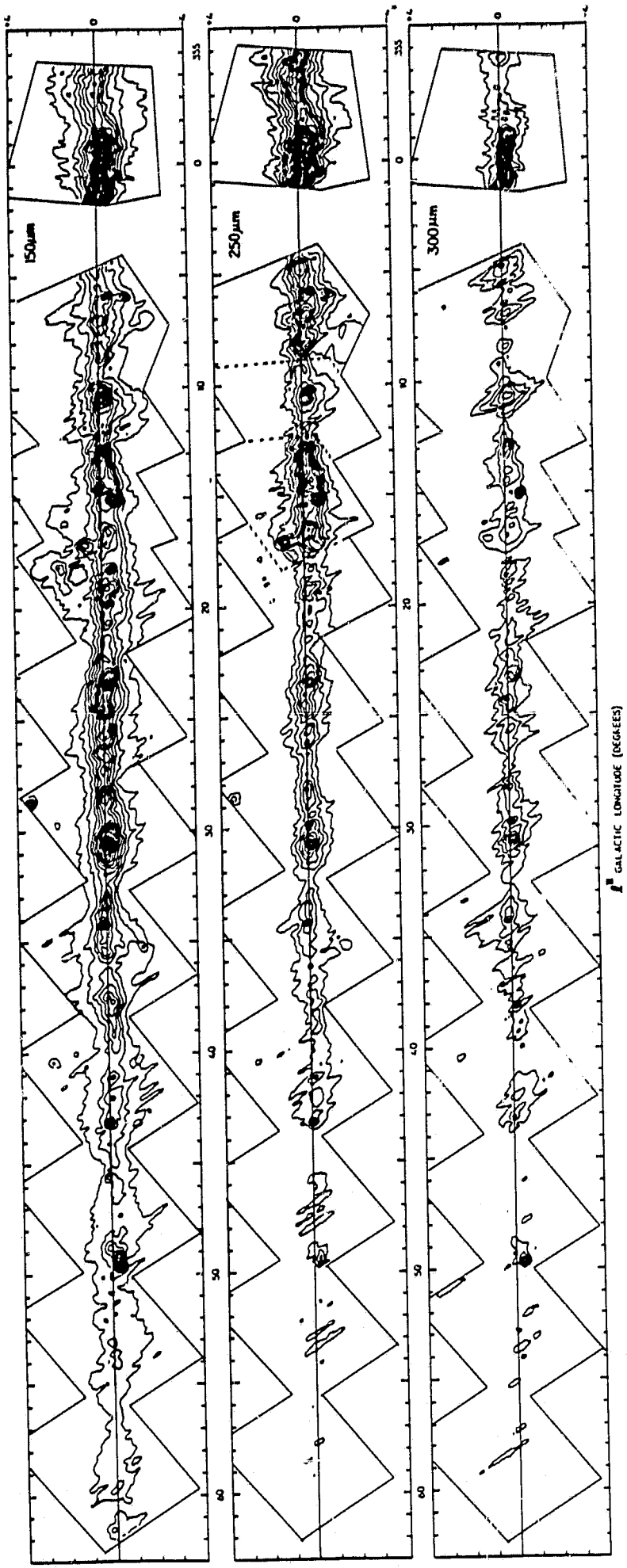

Figure 4

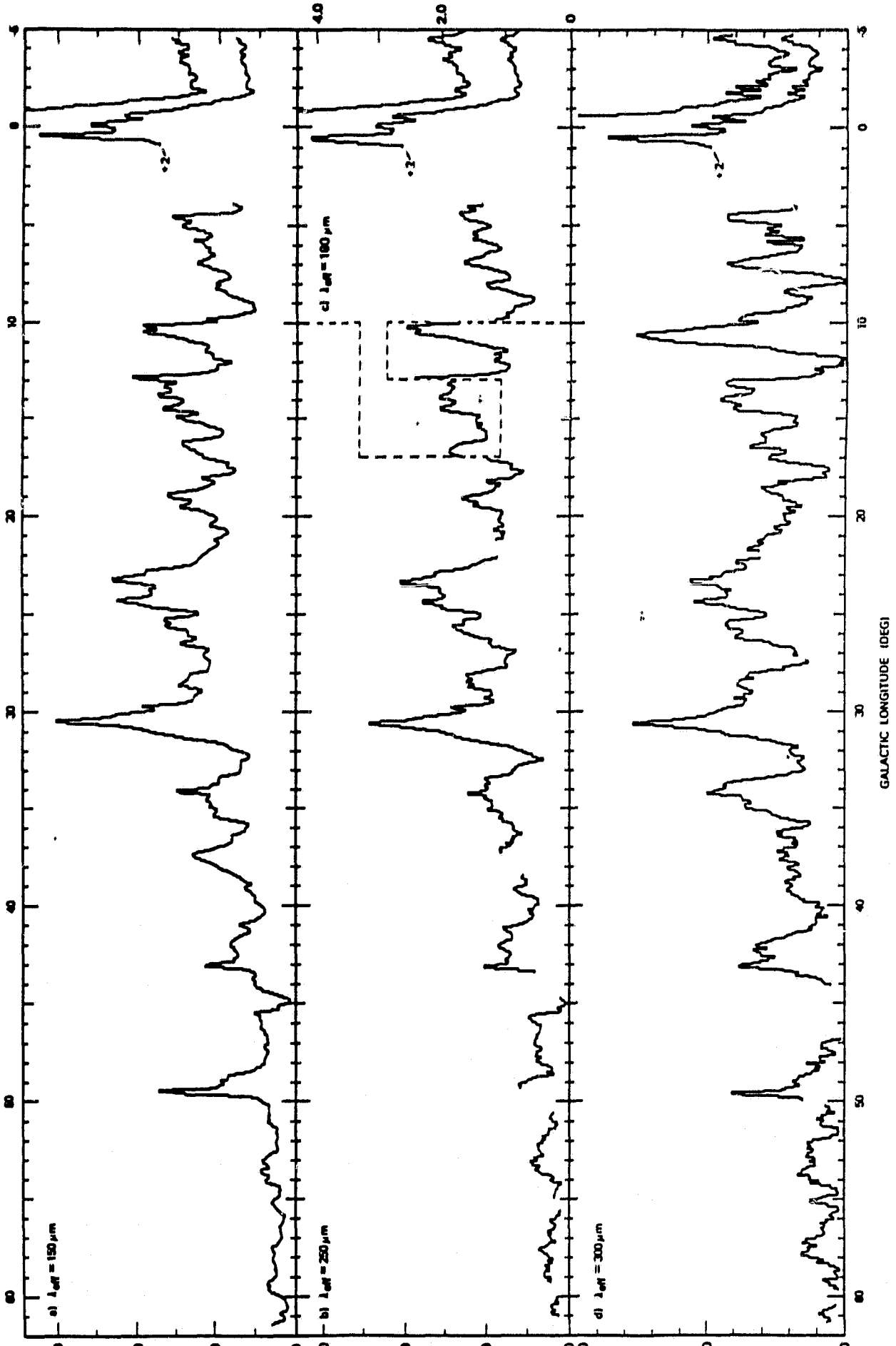

Figure 5

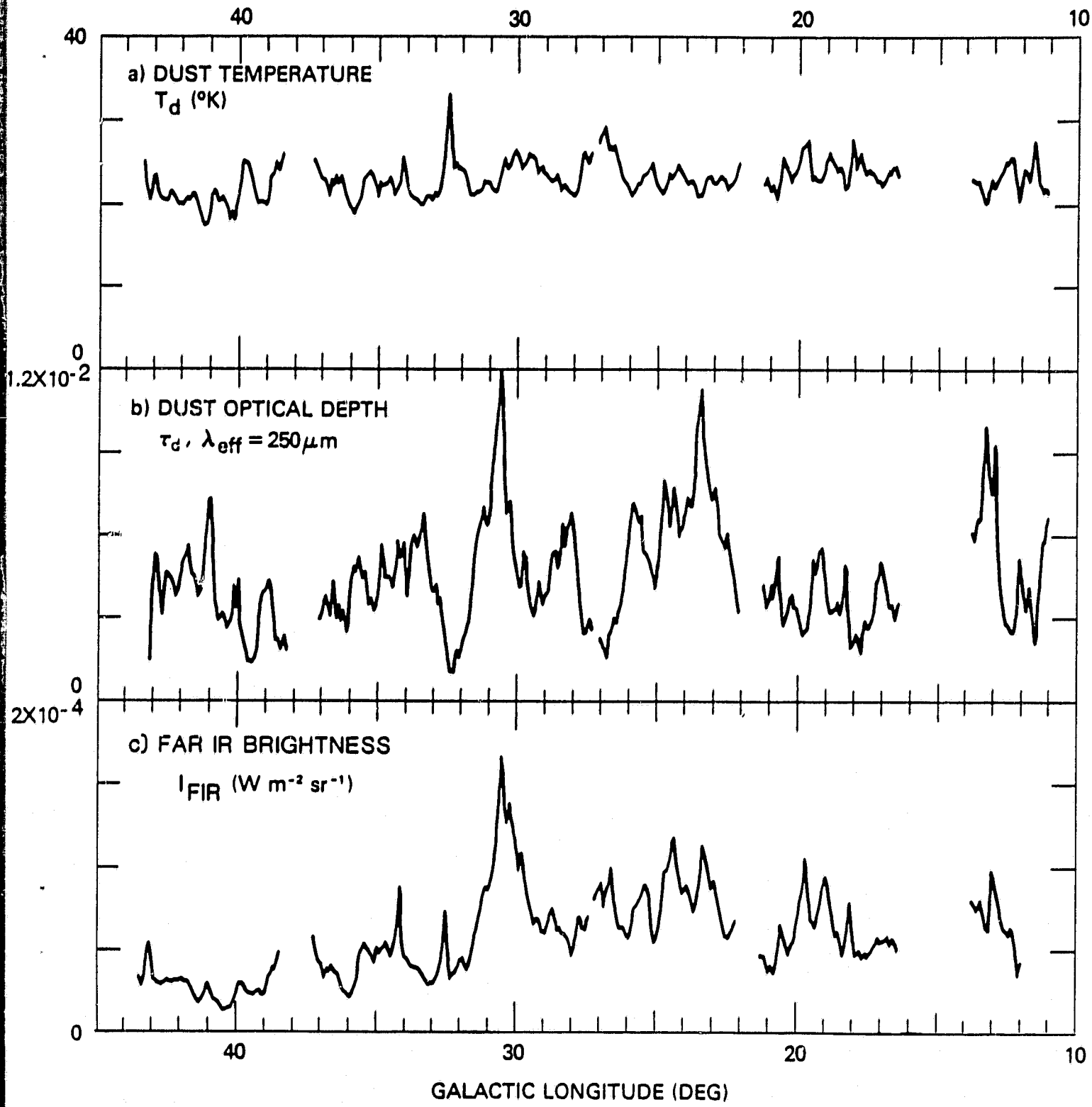

Figure 6

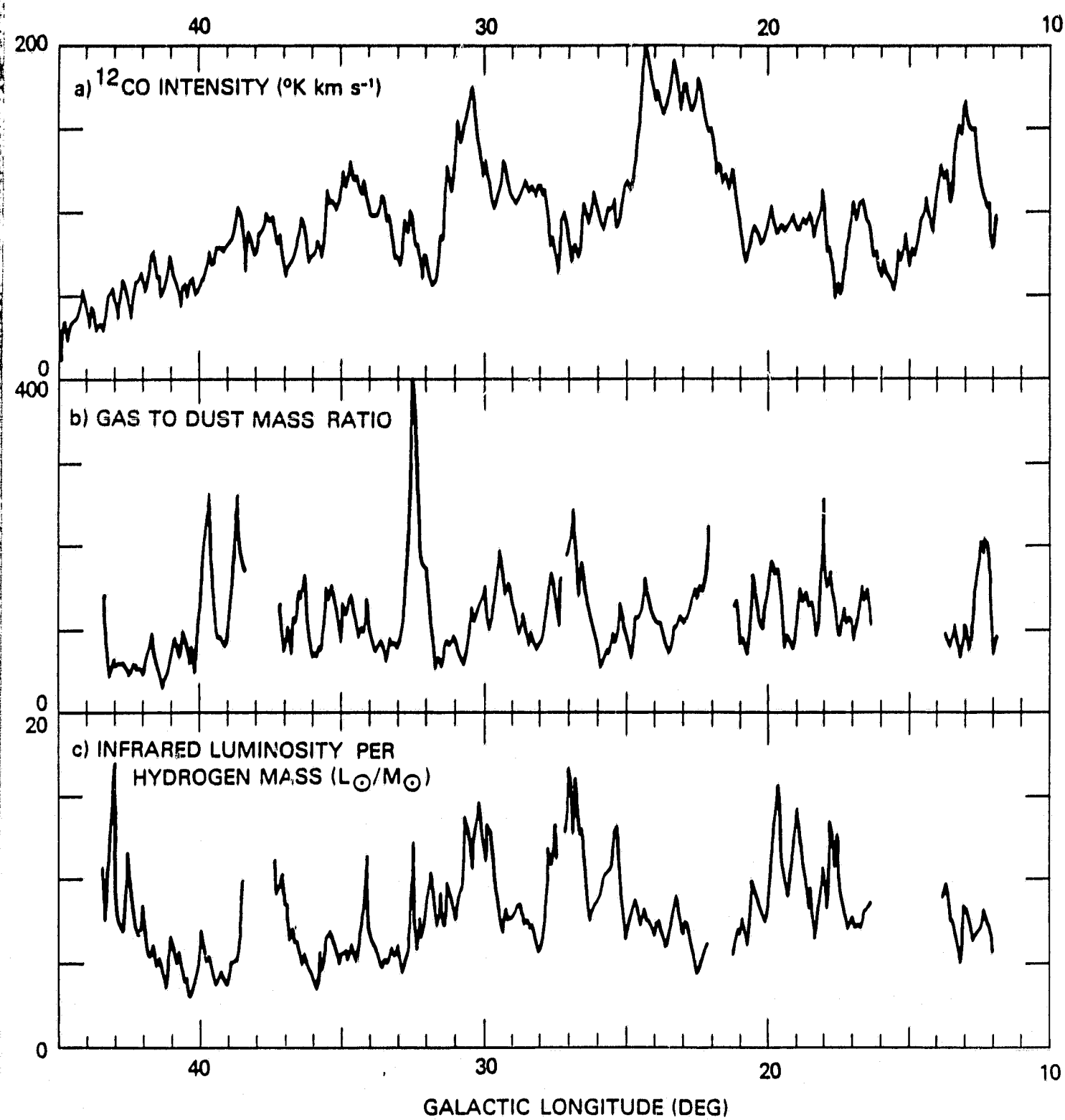

Postal addresses:

M. G. Hauser, R. F. Silverberg, T. Kelsall, D. Y. Gezari,

E. Dwek, D. Walser, J. C. Mather

Code 693.2

Laboratory for Extraterrestrial Physics

Goddard Space Flight Center

Greenbelt, MD 20771

L. H. Cheung

Gulf Research & Development Corp.

P. O. Box 37048

Houston, TX 77236

M. T. Stier

Perkin Elmer Corp.

Space Sciences Division

100 Wooster Heights Rd.

Danbury, CT 06810